RESTRICTED

COPY NO. 8

RM No. E8A29

UNCLASSIFIED

NACA

RESEARCH MEMORANDUM

ICE PROTECTION OF TURBOJET ENGINES BY INERTIA SEPARATION OF WATER

III - ANNULAR SUBMERGED INLETS

By Uwe von Glahn

Flight Propulsion Research Laboratory
Cleveland, Ohio

NATIONAL ADVISORY COMMITTEE FOR AERONAUTICS

WASHINGTON

June 8, 1948

UNCLASSIFIED RESTRICTED

NATIONAL ADVISORY COMMITTEE FOR AERONAUTICS

RESEARCH MEMORANDUM

ICE PROTECTION OF TURBOJET ENGINES BY INERTIA SEPARATION OF WATER

III - ANNULAR SUBMERGED INLETS

By Uwe von Glahn

SUMMARY

An investigation was made of annular submerged inlets designed to prevent the entrance of water into a turbojet engine in an icing condition. The results show that, in order to be effective in maintaining water-free induction air, the inlet gap must be extremely small with a high inlet-velocity ratio; ram-pressure losses consequently are high. For practical purposes, all inlets investigated admitted moderate quantities of water and a considerable amount of compressor-inlet screen icing was observed. Annular inlets are also aerodynamically unsuitable because of the severe mass-flow shifts occurring in the inlet at angles of attack.

INTRODUCTION

An inlet that prevents the entrance of water droplets while maintaining good aerodynamic characteristics constitutes a fundamental approach to the ice protection of turbojet engines. A nonramming inlet that may prevent the entrance of water into the engine is the submerged or flush inlet. Such inlets must maintain good ram-pressure recovery and at the same time exclude water. Recent research at Ames Aeronautical Laboratory on the submerged side-inlet-type or flush side-inlet-type air intake has shown that total-pressure recoveries of approximately 92 percent can be attained with a nonramming inlet and that the side inlets are comparatively unaffected by angle of attack.

The aerodynamic performance of annular submerged inlets is a function of the location of the inlet with respect to the surface static-pressure gradient, the boundary layer ahead of and in the inlet, the inlet-velocity ratio, the ramp and diffusion angles, and

the degree of surface flushness of the inlet lip. A small layer above a curved surface is free of water because of water deflection by the body (reference 1). If the small water-free layer is thick enough and additional separation is gained by a small inertia-separation effect at the inlet, the design of an ice-free inlet should be possible. At a large angle of attack, the bottom quarter of an annular inlet may be subject to direct impingement of water droplets.

Aerodynamic and preliminary icing studies were conducted in the 6- by 9-foot high-speed test section of the NACA Cleveland icing research tunnel on a one-half scale model of an annular submerged inlet for use with an axial-flow turbojet engine. The results are presented in terms of ram-pressure recovery, radial velocity profiles, and icing characteristics. The purpose of this investigation was to determine the general aerodynamic performance characteristics of several annular submerged inlets under icing conditions and to determine the extent to which water intake into the engine could be prevented by suitable inlet design. The aerodynamic results are shown in the form of ram-pressure recovery as a function of design inlet-velocity ratio, surface static-pressure plots around the inlet lips and ramp, and the radial profiles of velocity at the compressor-inlet section. Typical residual icing photographs of the nose, inlet lips, and compressor-inlet screen are also presented.

Symbols

The following symbols are used in this report:

H	total pressure with reference to test chamber, pounds per square foot
L	maximum cross-sectional height of duct at any section, inches
l	distance from outer duct wall to total-pressure tubes, inches
p	surface static pressure, pounds per square foot
p_0	free-stream static pressure with reference to test chamber, pounds per square foot
q	dynamic pressure, pounds per square foot

S pressure coefficient $1 - \left(\frac{p - p_0}{q_0}\right)$

V indicated airspeed, miles per hour

α angle of attack, degrees

η ram-pressure recovery $1 - \left(\frac{H_0 - H_2}{q_0}\right)$

Subscripts:

0 free stream

1 nacelle inlet

2 compressor inlet

av average

APPARATUS AND INSTRUMENTATION

The submerged-inlet nacelle investigated is shown in figures 1 and 2. All inlet models were mounted on the 21-inch-diameter afterbody used in the investigation of half-scale water-inertia separation inlets for an axial-flow turbojet engine developing 4000 pounds static thrust at sea level and having an 11-stage compressor, eight cylindrical burners, and a single-stage turbine. Aft of the compressor-inlet section the models were the same as the internal water-inertia separation nacelle (reference 2). Ahead of the compressor-inlet section, a screen of concentrically mounted wires of 0.062-inch diameter and 0.25-inch spacing was installed to serve as an icing indicator.

Aft of the compressor-inlet section the same instrumentation was used as in reference 2 to measure mass flow, velocity profiles, and ram-pressure recovery. Additional instrumentation for the setup consisted of plastic pressure-belt installations on the top and the bottom of the nose section and lip at the inlet.

The large overhang of the model nose necessitated supporting the nose section from the walls of the tunnel (fig. 2) in order to maintain an equal circumferential spacing of the inlet and also to prevent excessive nose vibration.

DESCRIPTION OF CONFIGURATIONS

The two basic submerged-inlet configurations and modifications to each are shown in figure 3. Coordinates for the basic configurations are given in table I. The external contours of the basic designs were based on the coordinates given in reference 4. The following table presents the minimum inlet areas and inlet-velocity ratios of the configurations investigated:

Configuration	Inlet area (sq in.)	Design inlet-velocity ratio
C-1	32.9	1.35
C-2	57.7	.77
D-1	51.5	.86
D-2	65.7	.67
D-3	90.5	.49

The design inlet-velocity ratios were based on the minimum cross-sectional area at the inlet and determined for an airspeed of 550 miles per hour and an engine air flow of 19.6 pounds per second at a pressure altitude of 40,000 feet.

The first configuration C-1 (fig. 3(a)) consisted of a submerged inlet located in the nacelle nose just ahead of the maximum diameter in order to take advantage of the favorable pressure gradient along the surface. The ramp angle was 17° and the lip was made with a simple 3/8-inch leading-edge radius. The large ramp angle was chosen in order to reduce the diffuser length from the inlet to the compressor-inlet section, although the large diffusion in such a short length was known to be detrimental to the aerodynamic characteristics. The inlet gap or area was purposely made small in order to provide high inlet-velocity and good water-inertia separation characteristics at the inlet.

A modification C-2 (fig. 3(b)) was made to configuration C-1, which consisted in moving the whole forward body 1.5 inches ahead, thus increasing the inlet area and in turn decreasing the rate of diffusion.

The second basic design D-1 (fig. 3(c)) consisted of a submerged inlet with the same outer contours over the nose section as C-1, but with a ramp angle of 9°. The decrease in ramp angle required an increased nacelle length, which permitted a reduction in the rate of diffusion. The inlet lip was redesigned to improve the flow into the inlet for a wider range of inlet-velocity ratios.

Two modifications were made to the basic design D-1. The first modification D-2 (fig. 3(d)) consisted in moving the forward body ahead 1.5 inches as for C-2. The second modification D-3 (fig. 3(e)) consisted in moving the forward body 4 inches ahead of the original location. The inlet lip was unchanged for all the modifications.

206

METHOD AND INVESTIGATIONS

The aerodynamic investigations were conducted with and without the compressor-inlet screen in place. The basic designs were aerodynamically investigated over a range of angles of attack from 0° to 8° whereas the modifications were investigated only at 0° angle of attack. All configurations were investigated over a range of engine air flows at a free-stream velocity of approximately 260 miles per hour for both aerodynamic and icing investigations.

Preliminary icing studies were made in a manner similar to those of reference 2 in which an effective droplet size of 12 to 15 microns was used at free air-stream total temperatures of approximately 22° F. The icing periods were of 10-minute duration after which photographs were taken of residual icing on the nose, inlet lip, and screen.

RESULTS AND DISCUSSION

Aerodynamic

In general, the aerodynamic characteristics of the submerged inlets investigated were unsatisfactory. The high ram-pressure recovery previously reported for submerged inlets in fuselage sides was not realized. Rough model surfaces and the supporting wires for the nose section may have contributed to excessive boundary-layer development at the inlet and this boundary layer may have affected the ram-pressure recovery. The ram-pressure recoveries of this investigation should not be taken as the best that can be attained with a submerged inlet.

Surface static-pressure distribution. - Typical pressure distributions in terms of the pressure coefficient S along the forward nacelle body surface and ramp ahead of the inlet opening and around the leading edge of the inlet lip for configurations C-1 and D-1 are shown in figure 4. The high-pressure coefficients around the inlet lip of design C-1 (fig. 4(a)) indicate extremely high velocities and

a low critical Mach number. The nacelle-surface pressures indicate the usual increase in local velocity over a body of revolution as the maximum diameter is approached. The pressure coefficients then decrease to a free-stream value at the start of the inlet ramp. At the inlet lip, the pressure coefficient again increases as the high inlet-velocity field is approached.

The inlet lip for design D-1 is of much better design than design C-1, as shown in figure 4(b), because the surface pressure coefficients are not as high as for design C-1; hence, the critical Mach number for this inlet is considerably increased. The nacelle-surface and ramp-pressure distributions of designs C-1 and D-1 are similar.

Ram-pressure recovery. - The ram-pressure recovery η was calculated as $1 - \left(\frac{H_0 - H_2}{q_0}\right)$ where the total-pressure difference is the integrated average ram-pressure recovery of all the aerodynamic-rake stations in the compressor section. Ram-pressure-recovery values for all configurations as a function of design inlet-velocity ratio at an angle of attack of 0° are presented in the following table:

Configuration	Design inlet-velocity ratio V_1/V_0	Ram-pressure recovery η	
		With screen	Without screen
C-1	1.35	0.48	0.52
C-2	.77	----------	.42
D-1	.86	.63	.65
D-2	.67	.55	----------
D-3	.49	.58	----------

The difference in ram-pressure recovery for configurations C-2 and D-1 was caused by the smaller ramp angle and the better inlet-lip design of D-1.

Velocity distributions. - Typical radial profiles of velocity with and without the compressor-inlet screens are shown in figure 5. With the screen in place, the velocity profile for C-1 at an angle of attack of 0° becomes more curved indicating increased pressure losses due to flow separation on the inlet ramp. Little change is noted at the same condition for configuration D-1. Increasing the

902

inlet area has a pronounced tendency to straighten out the velocity profile, as shown by configurations D-1, D-2, and D-3. At an angle of attack of 8°, the radial profiles of velocity at the sides and the bottom quarters of the nacelle became more uniform because of more direct entrance of the air.

A rapid decrease in mass flow through the top quarter of the model occurred at small angles of attack. At an angle of attack of 8°, no air entered the top quarter of the inlet and the resulting mass-flow shift would be detrimental to engine performance.

Icing

In general, all the configurations iced in a similar manner. At an angle of attack of 0°, the nose section iced heavily to about 5 inches rearward from the stagnation point and light ice formations continued aft 3 inches more.

Configuration C-1, which had the smallest inlet gap and the highest inlet velocity, had the least screen icing. The rate of icing was considerably less than for a direct-ram type of inlet. The screen ice was most noticeable on the screen brackets and near the nacelle wall of the inlet duct where the duct velocity was highest. When the forward body of the inlet was moved ahead for configuration C-2, external icing occurred similar to that for configuration C-1; heavier screen icing, however, was observed.

Typical icing photographs of configuration D-1 are shown in figure 6 at an angle of attack of 0°. Configuration D-1 iced in a manner similar to design C-1. The more uniform air flow in the D-1 inlet caused the screen to ice more uniformly in a radial sense than the C-1 screen. Configurations D-2 and D-3 showed the same general external icing characteristics as D-1. As the inlet area was increased, the screen icing became more severe. Typical screen icing observed on configuration D-3 is shown in figure 7.

SUMMARY OF RESULTS

The results of the investigation of annular submerged inlets indicate that the inlets are partly successful in separating the water droplets from the air. Unless extremely high inlet-velocity ratios and small inlet gaps are used, the inlet admits moderate quantities of water; hence the engine inlet will be subject to some impact icing, but the rate of icing will be considerably less than for a direct-ram type inlet.

The highest ram-pressure recovery attained for any configuration investigated was 65 percent at a design inlet-velocity ratio of 0.86 and an angle of attack of 0°. At angles of attack of 8°, no air entered the top quarter of the inlet and the resulting mass-flow shift would be detrimental to engine performance.

Flight Propulsion Research Laboratory,
National Advisory Committee for Aeronautics,
Cleveland, Ohio.

REFERENCES

1. Hills, B.: The Velocity Field and Paths of Raindrops Around a Symmetrical Aerofoil in an Incompressible Field. Tech. Note No. AERO 1303, R.A.E., Oct. 1943.

2. von Glahn, Uwe: Ice Protection of Turbojet Engines by Inertia Separation of Water. I - Alternate Duct System. NACA RM No. E8A27, 1948.

3. von Glahn, Uwe: Ice Protection of Turbojet Engines by Inertia Separation of Water. II - Single Offset-Duct System. NACA RM No. E8A28, 1948.

4. Becker, John V.: Wind-Tunnel Tests of Air Inlet and Outlet Openings on a Streamlined Body. NACA ACR, Nov. 1940.

TABLE I - NACELLE- AND SPINNER-CONTOUR COORDINATES WITH REFERENCE TO THE NACELLE LEADING EDGE AND CENTER LINE FOR BASIC CONFIGURATIONS C-1 AND D-1.

[i, inside contour and o, outside contour; all values in inches]

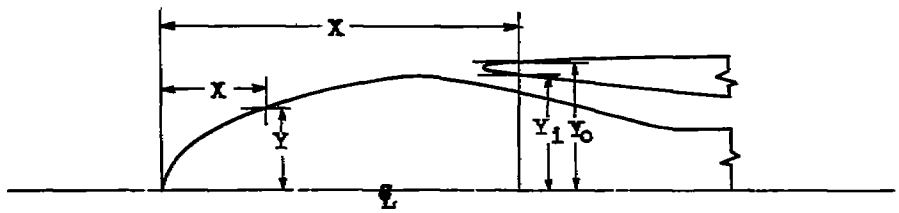

Forward body, C-1 design; leading-edge radius, 1.75							
X	Y	X	Y	X	Y	X	Y
0	0	7.82	6.37	15.82	8.59	23.82	9.44
1.82	2.93	9.82	7.03	17.82	9.00	26.32	8.85
3.82	4.40	11.82	7.62	19.82	9.34	37.82	5.00
5.82	5.50	13.82	8.15	21.82	9.56		

Inlet lip, C-1 design; leading-edge radius, 0.37								
X	Y_i	Y_o	X	Y_i	Y_o	X	Y_i	Y_o
26.81	9.82	9.82	30.18	- -	10.31	38.31	7.81	10.50
27.18	9.45	- -	32.18	- -	10.44			
28.18	- -	10.22	34.18	- -	10.50			

Forward body, D-1 design; leading-edge radius, 1.75							
X	Y	X	Y	X	Y	X	Y
0	0	9.82	7.03	19.82	9.34	24.82	9.25
1.82	2.93	11.82	7.62	20.82	9.50	48.51	5.06
3.82	4.40	13.82	8.15	21.82	9.53	49.51	5.00
5.82	5.50	15.82	8.59	22.82	9.50		
7.82	6.37	17.82	9.00	23.82	9.41		

Inlet lip, D-1 design; leading-edge radius, 0.19								
X	Y_i	Y_o	X	Y_i	Y_o	X	Y_i	Y_o
28.44	9.69	9.69	32.44	9.09	10.25	37.44	- -	10.47
29.94	9.44	9.97	33.44	9.00	10.34	38.44	- -	10.50
30.44	9.35	10.04	34.44	8.90	10.37	49.51	7.88	10.50
30.94	9.28	10.10	35.44	8.81	10.41			
31.44	9.22	10.16	36.44	- -	10.44			

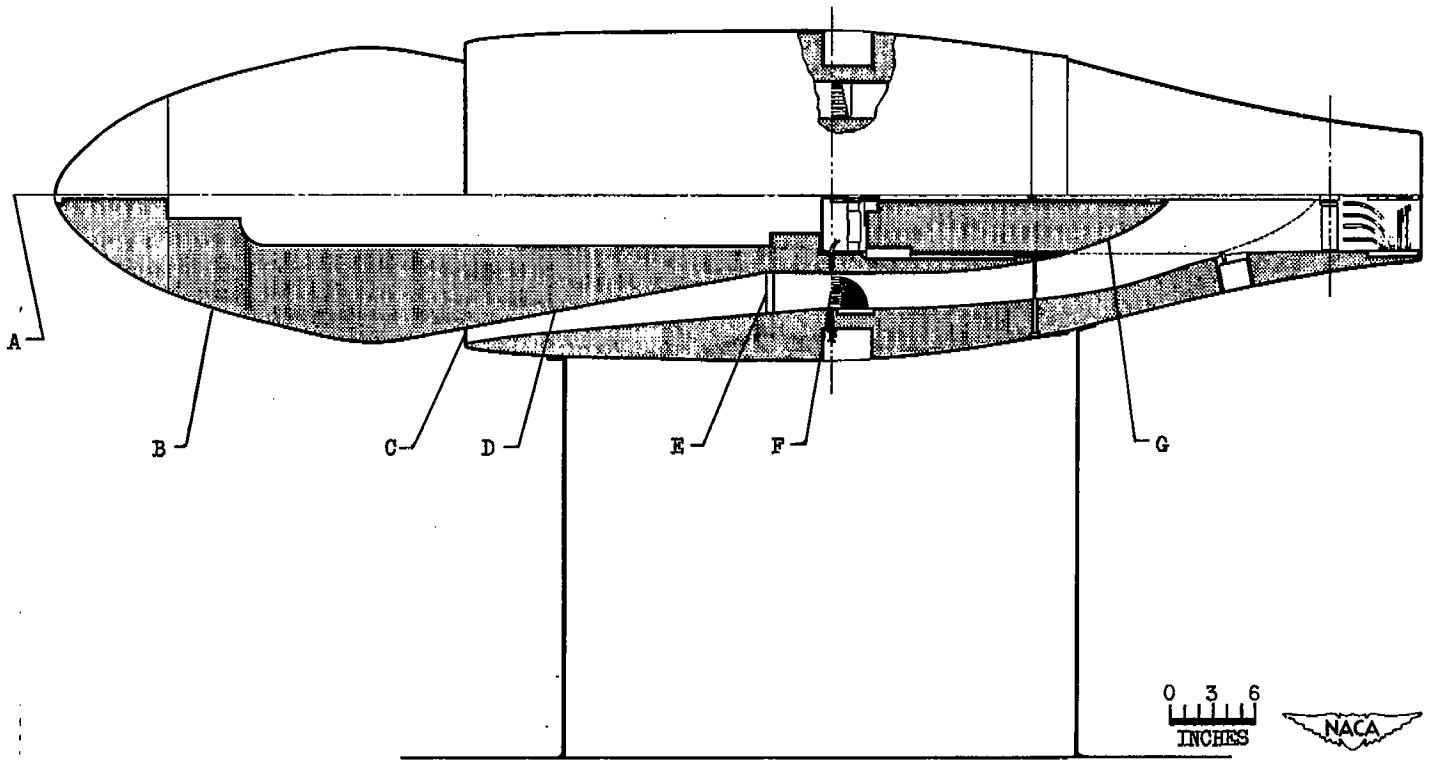

A Nacelle and tunnel center line
B Forward body
C Inlet lip
D Ramp
E Compressor-inlet screen
F Compressor-section instrumentation plane
G Air-flow control plug

Figure 1. - Schematic sketch of annular submerged-inlet setup showing configuration D-1.

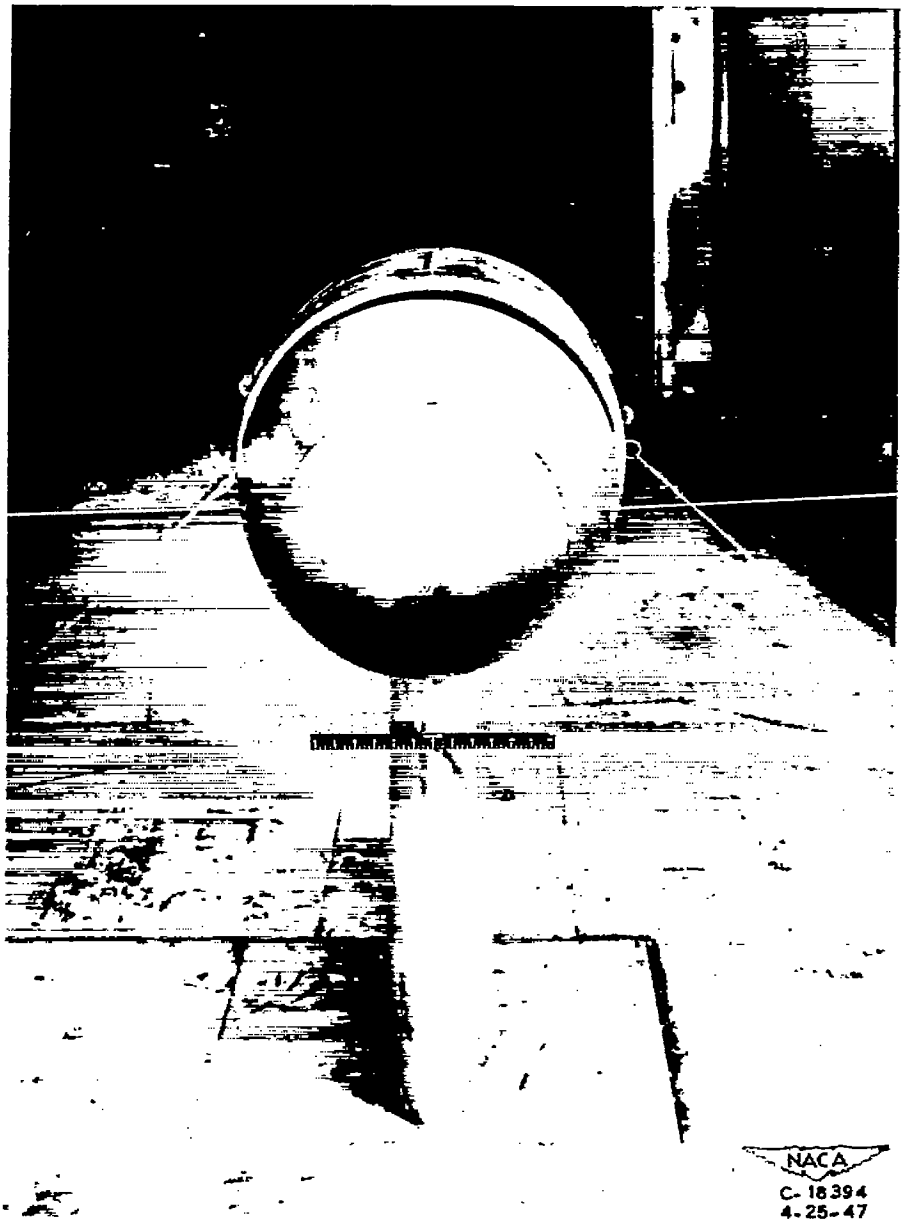

Figure 2. - Installation of typical annular submerged inlet in icing research tunnel.

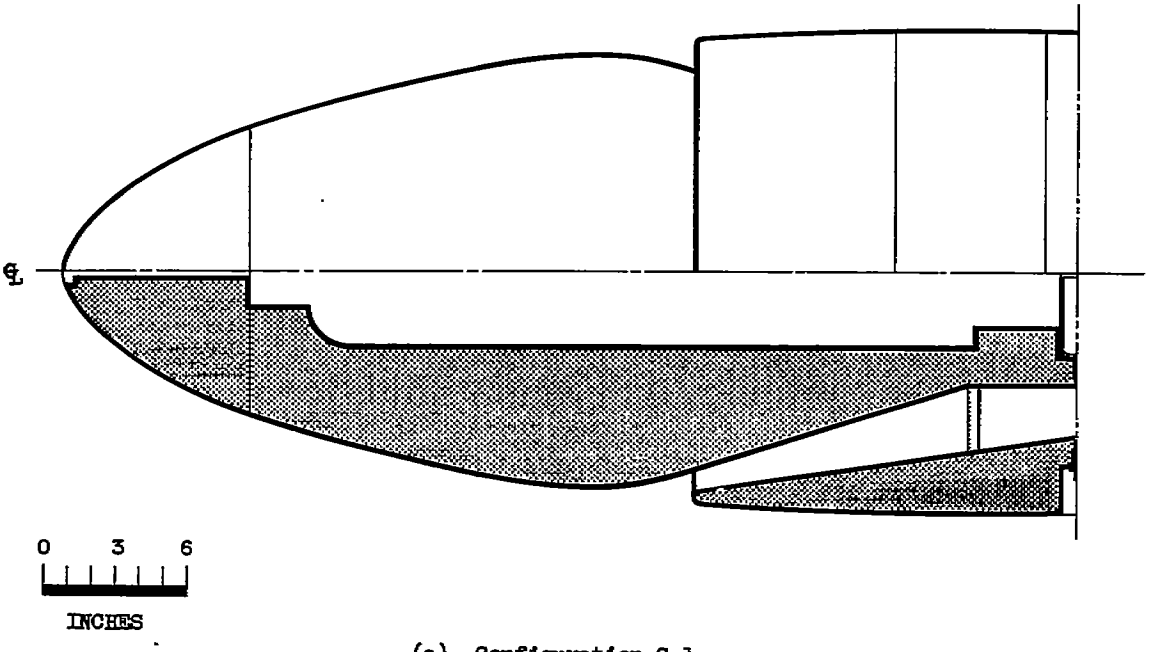

(a) Configuration C-1.

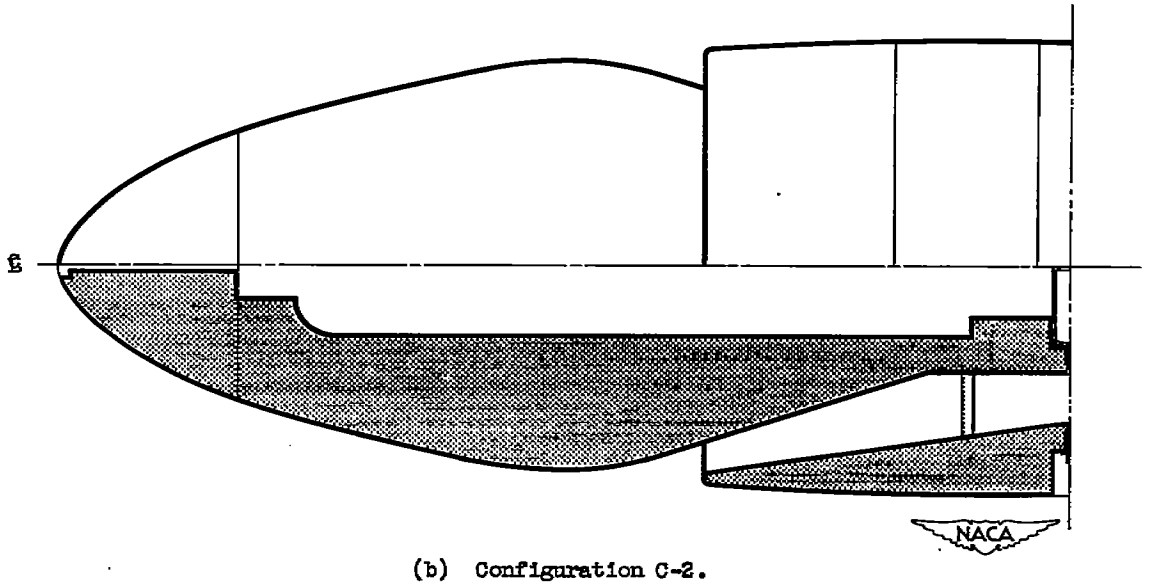

(b) Configuration C-2.

Figure 3. - Cross section of annular submerged inlets.

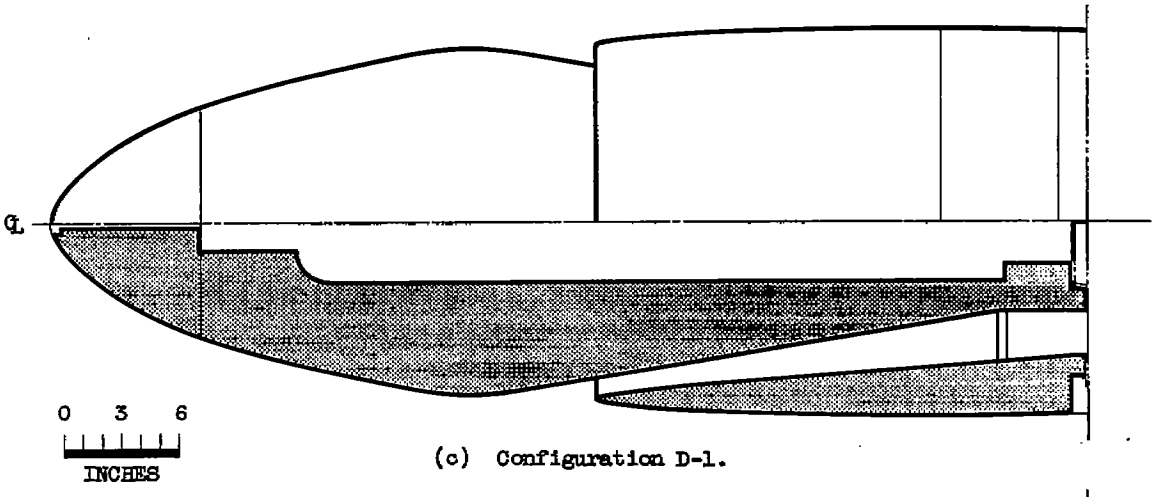

(c) Configuration D-1.

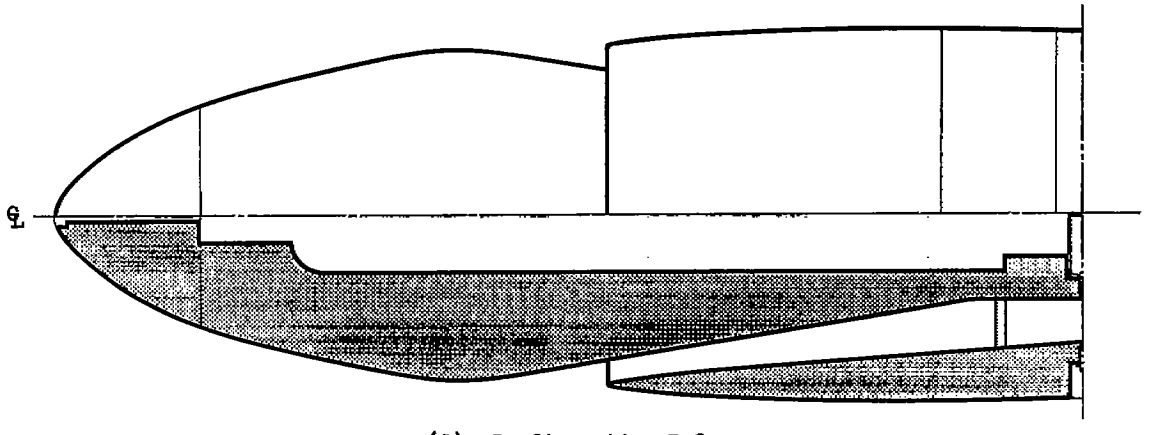

(d) Configuration D-2.

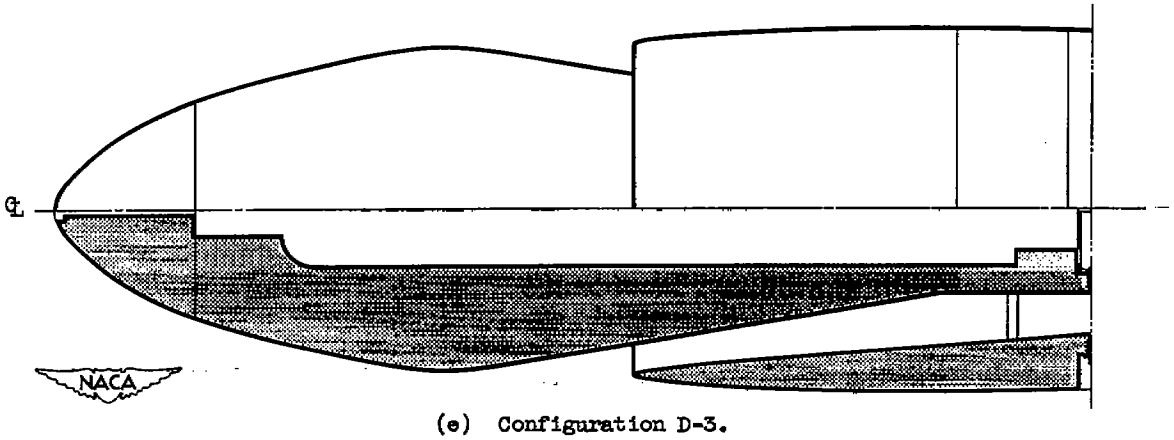

(e) Configuration D-3.

Figure 3. - Concluded. Cross section of annular submerged inlets.

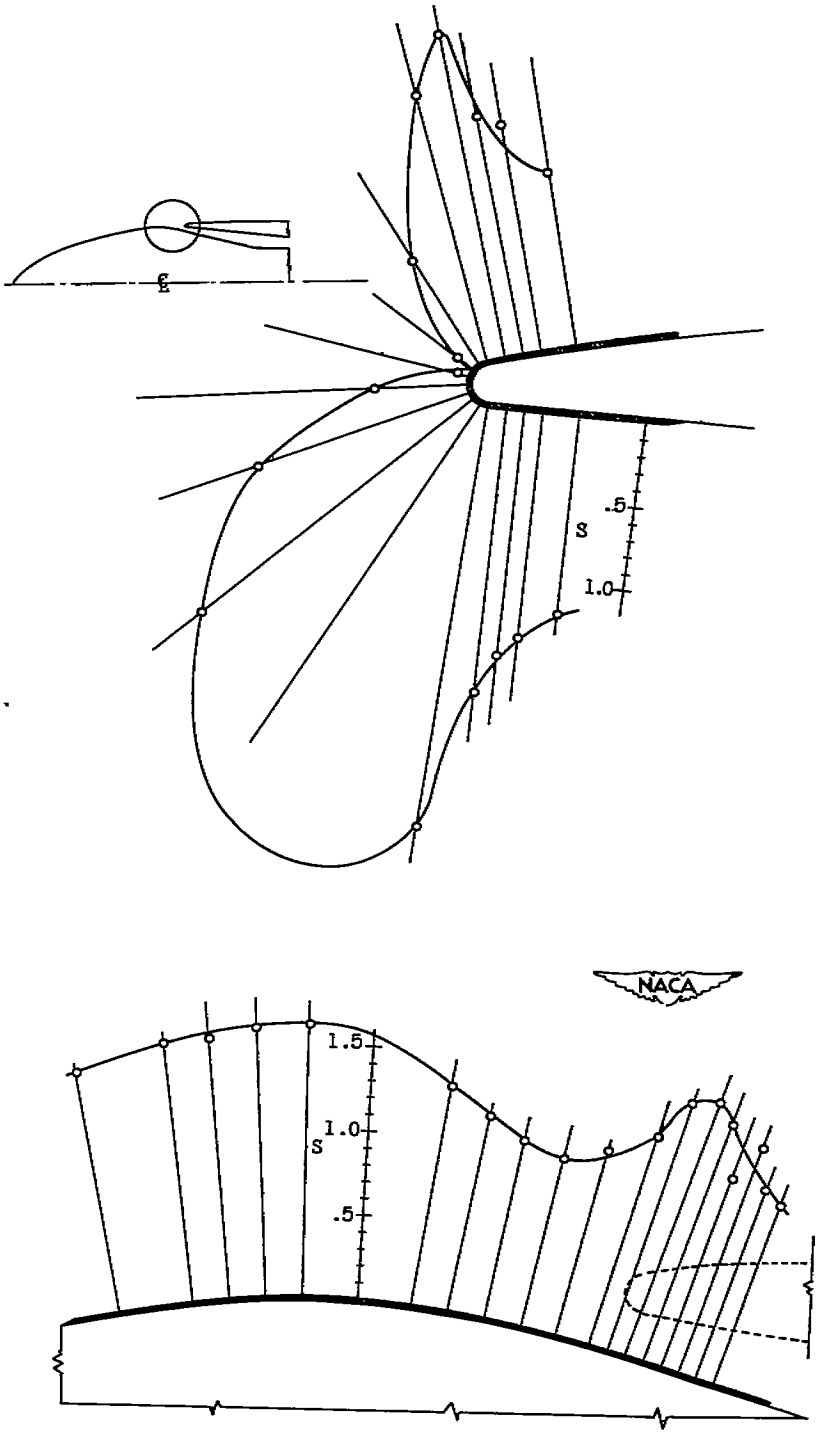

(a) Configuration C-1 with inlet-velocity ratio V_1/V_0 of 2.04.

Figure 4.- Typical surface pressure distribution around inlet lip and ramp. Airspeed V_0, 260 miles per hour; angle of attack α, 0°; maximum engine air flow.

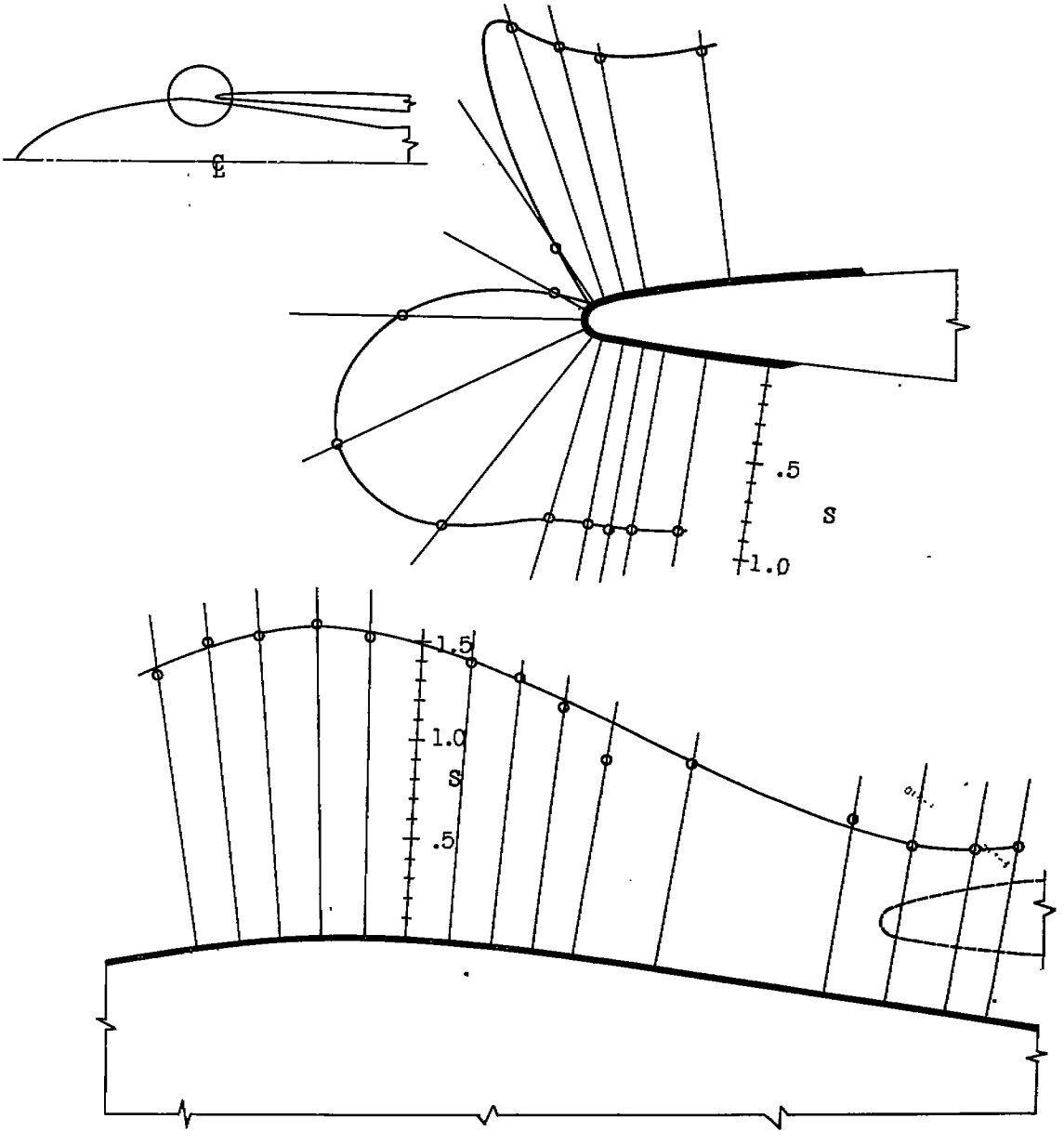

(b) Configuration D-1 with inlet-velocity ratio V_1/V_0 of 0.9.

Figure 4.- Concluded. Typical surface pressure distribution around inlet lip and ramp. Airspeed V_0, 260 miles per hour; angle of attack α, 0°; maximum engine air flow.

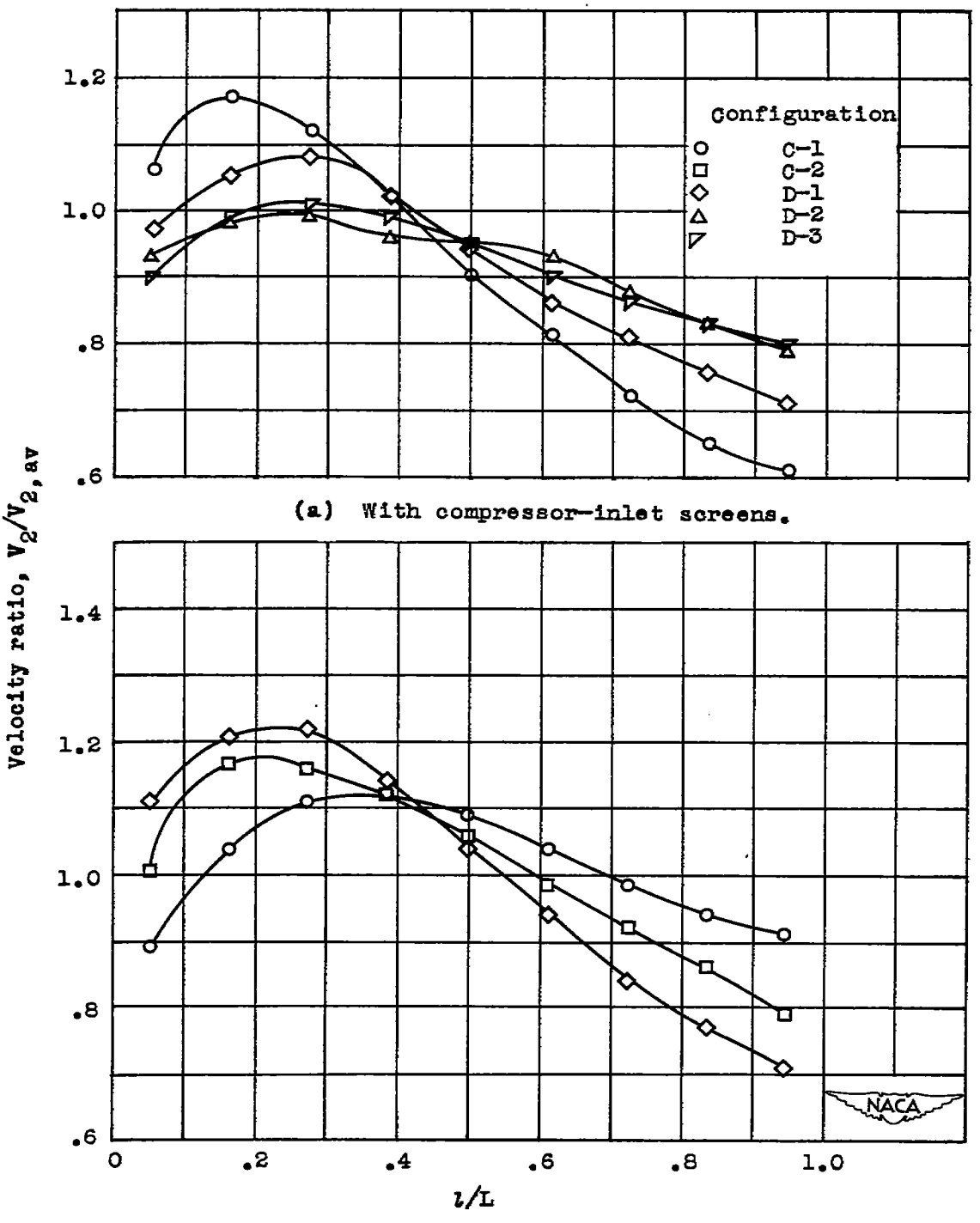

(a) With compressor-inlet screens.

(b) Without compressor-inlet screens.

Figure 5.- Typical radial profiles of velocity at compressor-inlet section for design inlet-velocity ratio. Air speed V_O, 260 miles per hour; angle of attack, 0°.

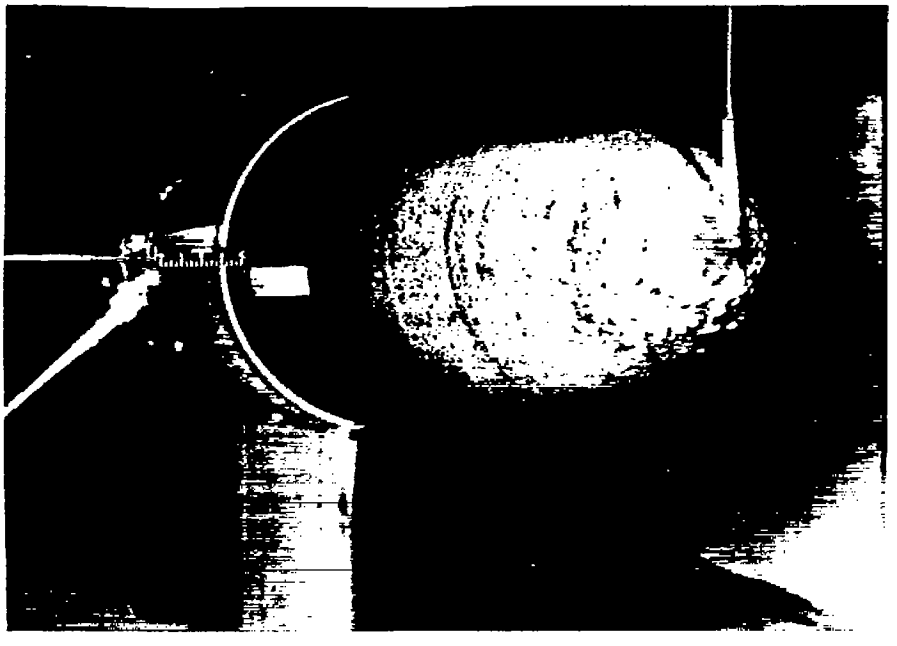

(a) Ice formations on nose.

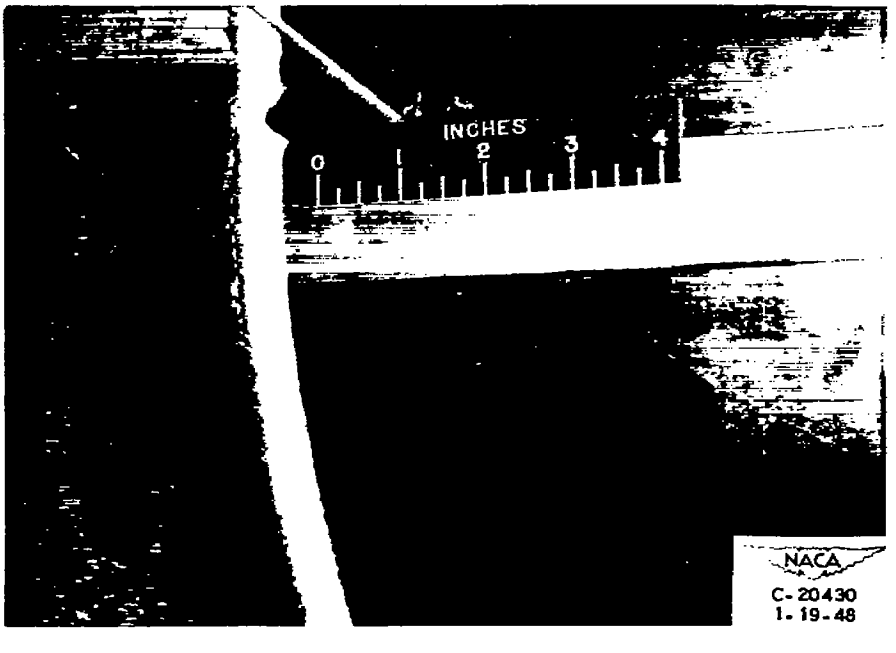

(b) Inlet-lip icing.

Figure 6. - Typical ice formations on configuration D-1. Airspeed V_0, 260 miles per hour; temperature, 22° F; angle of attack α, 0°; icing period, 10 minutes.

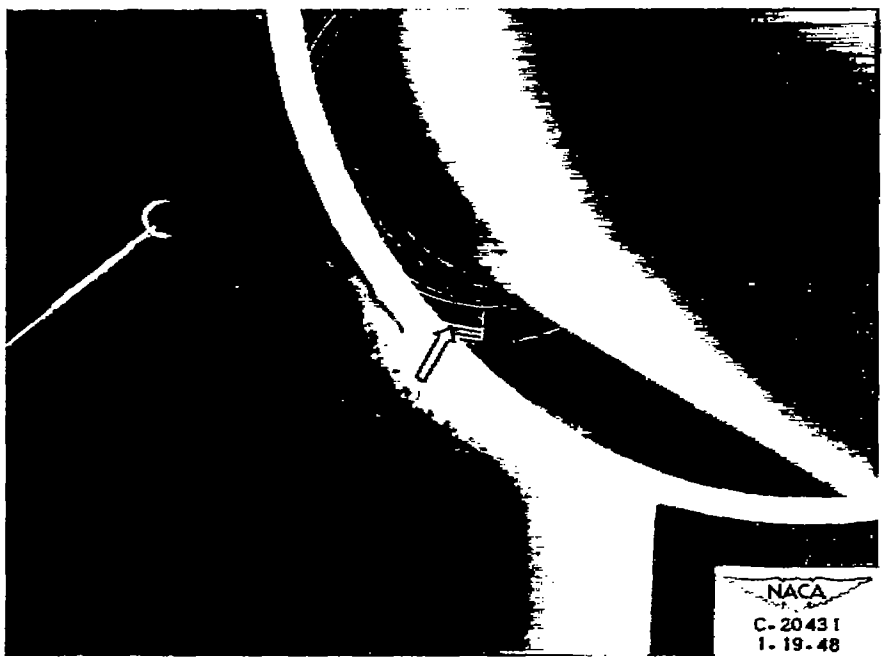

Figure 7. - Typical screen icing of configuration D-3. Airspeed V_0, 260 miles per hour; temperature, 22° F; angle of attack α, 0°; icing period, 10 minutes.